ELSEVIER

Journal of Molecular Catalysis A: Chemical 119 (1997) 19–33

JOURNAL OF MOLECULAR CATALYSIS A: CHEMICAL

Combining ab initio techniques with analytical potential functions. A study of zeolite–adsorbate interactions for NH_3 on H-faujasite

Martin Brändle, Joachim Sauer *

Max Planck Society, Research Unit "Quantum Chemistry" at the Humboldt University, Jägerstraße 10 / 11, D-10117 Berlin, Germany

Received 21 June 1996; accepted 12 September 1996

Abstract

A hybrid computational scheme which proved successful in the description of crystalline silica polymorphs is extended to the calculation of zeolite–adsorbate interactions. As a demonstrative application ammonia adsorption on H-faujasite at site III′ was investigated. The Hartree–Fock method (QM) is combined with shell model potentials (MM) based on ab initio data for the interaction of NH_3 and NH_4^+ with zeolites. This 'mechanical' embedding scheme accounts for the constraints imposed by the lattice on the structure relaxation at the reaction site. The long range contribution of the electrostatic potential of the crystal to the reaction energies is obtained from the MM energies of the host (periodic lattice) and of the embedded zeolite model. Although it converges slowly with increasing size of the embedded cluster, the total QM/MM energies are remarkably stable. The embedding scheme allows to use basis sets sufficiently large and flexible to describe both the neutral complex and the ion pair structures well. Ammonium ions in zeolites are therefore correctly described as more stable than ammonia. After including corrections for electron correlation, basis set superposition error, zero point energy and thermal contributions, the predicted estimate for the energy of formation of NH_4^+ from NH_3 and the acidic zeolite of 112 kJ/mol is in close agreement with the range of heats of adsorption inferred from microcalorimetry and temperature-programmed desorption of ammonia on H-faujasites.

Keywords: Faujasite; Ammonia adsorption; Shell model potential; Mechanical embedding; Ab initio method

1. Introduction

Protonated zeolites are widely used in heterogeneous catalysis, e.g. in the conversion of hydrocarbons or in the methanol-to-gasoline process. Since the first step involves adsorption of a molecule on a catalytically active site, here a Brønsted acidic hydroxyl group Si–O(H)–Al, adsorption has been widely investigated with experimental and quantum chemical methods [1,2]. So far, several ab initio quantum chemical studies of adsorption of small molecules have been undertaken adopting cluster models cut out from the zeolite and saturated with hydrogen atoms [1,3–14]. The cluster model, however, involves several approximations. First, fully structurally relaxed gas phase clusters of small to medium size do not reflect a specific framework structure with respect to the same atoms in

* Corresponding author. Tel. +49-30-20192300; fax: +49-30-20192302; e-mail: js@qc.ag-berlin.mpg.de.

PII S1381-1169(96)00497-9

a connected framework. This distortion may even be exaggerated because the saturator atoms are able to form intramolecular hydrogen bonds. Second, long range electrostatic interactions which are slowly convergent with increasing cluster size are neglected [3,15]. Ideally, periodic ab initio calculations [16] could account for both structure and long range effects. Up to now they have been restricted to ammonia adsorption on a rigid chabazite framework with a small unit cell [15,17,18]. To make the calculations feasible, a minimal basis set had to be applied with the consequence [1] that contrary to experimental evidence the proton did not transfer to ammonia. Another approach are periodic pseudopotential plane wave calculations, applications of which to adsorption of water and methanol in zeolites were reported recently [19–21]. Because of the huge number of plane waves to be held in memory, these methods are also limited up to now to zeolites with small unit cells, e.g. sodalite and chabazite.

Such limits are overcome by embedding the cluster either electronically or mechanically into its environment. Electronic embedding techniques have been suggested at various levels. They rely on Green's function techniques (implemented in the EMBED code [22–24]), add the external electrostatic potential (ESP) of the crystal in terms of multipole expressions to the Fock matrix of the cluster [17,18], embed the cluster into a finite set of point charges fitted to the ESP [25,26] or into a lattice of point charges [27] estimated from population analysis of cluster calculations or from chemical considerations. Merits and limits of the different approaches were discussed in Ref. [1]. Applications mainly treated ammonia sorption in zeolites [17,18,25–28].

In hybrid quantum mechanical/molecular mechanical methods the embedding environment is described by an analytical potential function (Pot) and the site of interest by a quantum chemical method (QM). We apply a 'mechanical' embedding scheme which proved successful in the description of the structures of silica polymorphs [29] and of Brønsted acidic zeolites [30] to adsorption in zeolites now. We make the assumption that the structure of the environment can be accurately modeled by analytical potential functions. The structures of both the environment and the reaction site are completely relaxed, which has the advantage that the framework can accommodate to the structural distortions induced by the interaction of a molecule with the adsorption site. The present embedding scheme includes approximately the long range contribution to the adsorption energy, but polarization of the electronic distribution of the reaction site by the electrostatic potential of the environment is not accounted for. However, due to changes of the structure the wavefunction of the quantum part, the embedded cluster, is also different from that of a free cluster.

As a demonstrative application we choose ammonia adsorption in faujasite since ammonium-exchanged faujasites are well characterized experimentally. From the ammonium-exchanged form the acidic zeolite is obtained by desorbing ammonia and water at elevated temperatures. The same process is employed in temperature-programmed desorption experiments to characterize the acidity of zeolites. The reverse process, adsorption of ammonia onto the proton form of the zeolites, is applied in microcalorimetry. The measured heats of desorption or adsorption are collective and averaged properties which include many factors like, e.g., the nature and number of the binding sites, their accessibility and local structure, and they depend therefore on the pretreatment of the zeolite and the temperature at which the experiments are carried out. Usually, these thermochemical techniques are combined with spectroscopic methods as IR and solid state NMR to identify the nature of the acid sites involved [2,31]. The location of ammonia and ammonium ions in faujasite is revealed by ^{1}H MAS NMR spectroscopy in combination with IR spectroscopy and neutron diffraction [32]. The faujasite structure and its sites are shown in Fig. 1. Ammo-

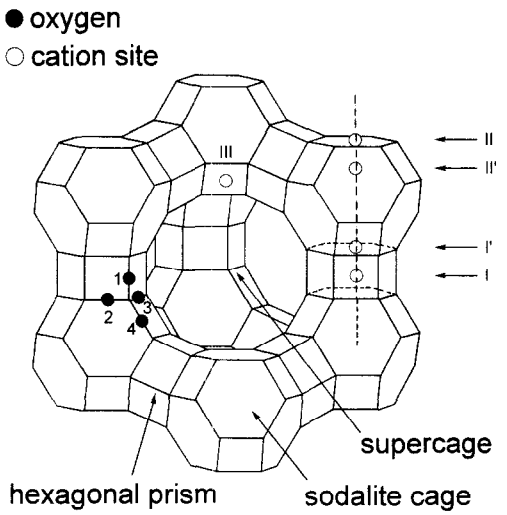

Fig. 1. The faujasite structure. The different oxygen positions are numbered from 1–4. The cation sites are indicated by Roman numerals. Site III′ involves coordination to O1 and O4.

nium ions are mostly found in the sodalite cage at sites I′ and II′ involving coordination to the oxygen atoms O_2 and O_3, and in the supercage, probably at site III′ involving coordination to O_1 and O_4. We will deal with ammonia adsorption at site III′.

2. Method

2.1. The embedding scheme

The embedding scheme applied [10,29] partitions the entire system (S) into two parts, the inner region (I) and the outer region (O). S = I + O. The inner region is the part of chemical interest and is treated quantum mechanically. The outer part is described by analytical potential functions. If the inner part is chemically bonded to the outer region, the partitioning leads to dangling bonds which are saturated with hydrogen atoms, the so-called link atoms. The inner part (I) and the link atoms (L) then form the cluster, C = I + L. The energy of the entire system is obtained by a subtraction scheme:

$$E(\mathrm{S}) = E_{\mathrm{QM}}(\mathrm{C}) + E_{\mathrm{Pot}}(\mathrm{S}) - E_{\mathrm{Pot}}(\mathrm{C}) + \Delta \quad (1)$$

with

$$\Delta = -E_{\mathrm{QM}}(\mathrm{L}) - E_{\mathrm{QM}}(\mathrm{I\text{–}L}) + E_{\mathrm{Pot}}(\mathrm{L}) + E_{\mathrm{Pot}}(\mathrm{I\text{–}L}) \quad (2)$$

it is assumed that $\Delta = 0$, which is fulfilled in the limiting case that the analytical potential function ideally mimics the quantum mechanical potential energy surface of the cluster. Hence, this scheme works the better the tighter the analytical potential function follows the quantum mechanical potential energy surface. Fitting of analytical potential functions is therefore a substantial part of the work. Note that by way of Eq. (1) we eliminate any double counting of contributions due to the potential and the quantum mechanical calculations and at the same time the influence of the link atoms which are not part of the real solid.

Note also that there is no direct influence of the charge distribution of the outer part on the wavefunction of the cluster. The latter is different from the wavefunction of a gas phase cluster only by way of the structure changes the cluster experiences when it is embedded in the outer part.

From Eq. (1) the following relations are obtained for the forces on the nuclei:

$$F_\alpha(\mathrm{S}) = F_{\alpha,\mathrm{QM}}(\mathrm{C}) + F_{\alpha,\mathrm{Pot}}(\mathrm{S}) - F_{\alpha,\mathrm{Pot}}(\mathrm{C}) \quad | \quad \alpha \in \mathrm{I}$$
$$F_\beta(\mathrm{S}) = F_{\beta,\mathrm{Pot}}(\mathrm{S}) \quad | \quad \beta \in \mathrm{O} \quad (3)$$

The force that acts on an atom α in the inner region is a contribution of three terms: The force obtained by a quantum mechanical calculation of the cluster, and the molecular mechanics forces calculated for the host and the cluster, respectively. For an atom β of the outer region, the force is given by the molecular mechanics expression for the host alone. These forces are then used in a structure optimization procedure. The link atoms are not moved according to the forces acting on them. Their position $\boldsymbol{r}_{\mathrm{H}}$ is given as a function of the atoms of the real

system, r_O and r_{Si}, which they link, $r_H = f(r_O, r_{Si})$. In practice they are put on the Si–O bond axes at a given distance from the outmost O atom of the inner part. The residual forces on the link atoms make contributions to the forces on the real atoms which they link [29].

The results this 'mechanical' embedding scheme [29] yields for the adsorption of molecules at active sites in zeolites differ from gas phase cluster calculations in two respects:

(1) the relaxation of the nuclei on interaction is constrained when the cluster is part of the zeolite lattice;

(2) the long range electrostatic contributions are obtained from the potential function used.

2.2. Decomposition of the adsorption energy

The energy of adsorption of a molecule B on the zeolite Z is defined as

$$\Delta E = E(Z \cdot B) - E(Z) - E(B) \tag{4}$$

If Z is modelled by a cluster C and all systems in Eq. (4) are optimized by a quantum chemical method we obtain the adsorption energy of the free space cluster $\Delta E_{QM//free}(C)$.

If we apply the embedding scheme for both Z · B and Z we obtain by inserting Eq. (1) into Eq. (4)

$$\begin{aligned}\Delta E &= E_{QM}(C \cdot B) + E_{Pot}(S \cdot B) - E_{Pot}(C \cdot B) \\ &\quad - E_{QM}(C) - E_{Pot}(S) + E_{Pot}(C) - E_{QM}(B) \\ &= \Delta E_{QM}(C) + E_{Pot}(S \cdot B) - E_{Pot}(S) \\ &\quad - (E_{Pot}(C \cdot B) - E_{Pot}(C)) \\ &= \Delta E_{QM//Emb}(C) + \Delta E_{Pot//Emb}(S) \\ &\quad - \Delta E_{Pot//Emb}(C) = \Delta E_{QM//Emb}(C) \\ &\quad + \Delta E_{LR//Emb}\end{aligned} \tag{5}$$

The notations 'QM//Emb' and 'Pot//Emb' mean that the respective interaction energies are now defined for the equilibrium structures of Z · B and Z obtained with the 'mechanical' embedding scheme. The difference $\Delta E_{QM//Emb} - \Delta E_{QM//free}$ represents the change of the adsorption energy due to the limited structural relaxation of the embedded cluster compared with the free cluster. We have defined

$$\begin{aligned}\Delta E_{LR//Emb} &= \Delta E_{Pot//Emb}(S) \\ &\quad - \Delta E_{Pot//Emb}(C)\end{aligned} \tag{6}$$

In order to see the physical meaning of this term we analyze it in terms of energy contributions of the inner, outer and link regions and their interactions (neglecting three body terms). A notation like I//S · B means a contribution from the internal part only calculated at the structure of the whole system (periodic zeolite) in the presence of the adsorbed molecule. Contributions from interactions between two regions are denoted, e.g. I–O//S · B or L–B//S · B. Since

$$S = I//S + O//S + I\text{–}O//S \tag{7a}$$

$$C = I//S + L//S + I\text{–}L//S \tag{7b}$$

$$\begin{aligned}S \cdot B &= I//S \cdot B + O//S \cdot B + I\text{–}O//S \cdot B \\ &\quad + B//S \cdot B + I\text{–}B//S \cdot B \\ &\quad + O\text{–}B//S \cdot B\end{aligned} \tag{7c}$$

$$\begin{aligned}C \cdot B &= I//S \cdot B + L//S \cdot B + I\text{–}L//S \cdot B \\ &\quad + B//S \cdot B + I\text{–}B//S \cdot B \\ &\quad + L\text{–}B//S \cdot B\end{aligned} \tag{7d}$$

we obtain

$$\begin{aligned}S \cdot B - S + C - C \cdot B &= O//S \cdot B - O//S \\ &\quad + I - O//S \cdot B - I - O//S \\ &\quad + L//S - L//S \cdot B \\ &\quad + I - L//S - I - L//S \cdot B \\ &\quad + O - B//S \cdot B - L - B//S \cdot B\end{aligned} \tag{8}$$

Under the assumption that the outer and link regions of the system with and without the adsorbed base are the same (O//S · B = O//S and L//S · B = L//S) and that the structural distortion of the inner region is small when a

molecule adsorbs (I–O//S · B = I–O//S and I–L//S · B = I–L//S) we obtain

$$\Delta E_{\mathrm{LR}\,//\,\mathrm{Emb}} = E_{\mathrm{Pot}\,//\,\mathrm{Emb}}(\mathrm{O{-}B}) - E_{\mathrm{Pot}\,//\,\mathrm{Emb}}(\mathrm{L{-}B}) \quad (9)$$

The cluster should be always large enough to include all short range interactions between the adsorbed molecule and the zeolite within the I–B part. Hence, O–B and L–B include only long range contributions and this justifies to consider $\Delta E_{\mathrm{LR}//\mathrm{Emb}}$ defined by Eq. (6) as long range correction to the interaction energy. For large enough clusters $E_{\mathrm{Pot}//\mathrm{Emb}}$(L–B) vanishes and therefore

$$\Delta E_{\mathrm{LR}\,//\,\mathrm{Emb}} \approx E_{\mathrm{Pot}\,//\,\mathrm{Emb}}(\mathrm{O{-}B}) \quad (10)$$

2.3. Details of the quantum mechanical calculations

All energy and gradient calculations for the cluster were performed in the Hartree–Fock approximation using the program system TURBOMOLE [1] [33]. For silicon, aluminum, and hydrogen basis sets of double zeta plus polarization (DZP) quality were used. For the oxygen and nitrogen atoms a triple zeta plus polarization (TZP) basis set was applied. For the Si, Al/O, N/H atoms the (11s, 7p)/(9s, 5p)/(4s) Gaussian basis sets were taken from Huzinaga [34,35] contracted into the pattern {521111, 4111}/{51111, 311}/{31}. Polarization functions were added with exponents 0.4 (Si), 0.3 (Al), 1.2 (O), 1.0 (N), and 0.8 (H). The cutout was made such that the clusters terminate with OH groups. If the oxygen atom of the terminating OH group was bonded to a silicon atom a fixed link atom distance r_{OH} of 94.5 pm was used. In the case of aluminum it was set to 94.0 pm. This value was obtained by free cluster optimizations with the same basis set. All SCF calculations were carried out in C_1 symmetry.

[1] TURBOMOLE is commercially available from Molecular Simulations Inc., San Diego, CA.

2.4. Potential functions used

For the potential calculations we use an ion-pair potential that adopts the shell model introduced by Dick and Overhauser [36]. In this approach, an ion, e.g. the O^{2-} ion in silicates, is represented by a pair of point charges, the positive core and the negative massless shell that are connected by a harmonic spring. It is often applied to the negative ions only, because of their larger polarizability. The sum of the core and shell charges is the formal charge of the anion. The electrostatic energy is evaluated for all cores and shells and the shell positions are optimized to yield the lowest energy. Non-bonded repulsion terms are added, mostly between oppositely charged ions.

An important aspect is the use of potential functions that have been parametrized on ab initio data obtained at the same level of approximation as employed for the quantum mechanical calculation of the cluster in order to maintain consistency [29]. Such a data base for silica and zeolites has been generated by Hill and Sauer [37,38] and used to parametrize a shell model ion-pair potential [39]. It is in fact unavoidable to use ab initio data for the fitting, since the embedding scheme also requires shell model calculations on the clusters saturated with hydrogen atoms. Empirically parametrized shell model potentials cannot provide parameters for these terminating atoms that are missing in the real solid.

The ab initio shell model ion-pair potential for zeolites derived by Schröder and Sauer [39] assumes formal charges on the ions and Born–Mayer repulsive terms between oppositely charged ions. Its good performance suggests to extend this potential function Ansatz in the same manner to zeolite–adsorbate interactions although small molecules do not seem to be the natural case of application. On the other hand, when the cluster is sufficiently large, the only part of the potential showing up in the final results are the electrostatic properties. The shell model potentials derived below for NH_3/NH_4^+

are mainly designed for embedding calculations and for getting reasonable start structures.

The shell model potential fits followed the same procedure as described earlier [37]. Ab initio data bases of equilibrium and distorted zeolite–adsorbate models as well as of the ammonia and ammonium ions were generated. The structures used for the fits are listed in Table 1. All zeolite–adsorbate models were terminated with hydroxyl groups. Both force constants at equilibrium structures and energy gradients at equilibrium and distorted structures were considered in the fits. Energies were not used. The atom types for the interaction potentials of NH_3 and NH_4^+ with zeolites are shown in Fig. 2. The potential parameters were evaluated in a multi step procedure, starting with the determination of the intramolecular potentials of the adsorbates. Since it was not possible to determine core–shell interaction parameters for the nitrogen atom in NH_4^+, two separate potentials for the NH_3 and NH_4^+ interaction had to be developed. The consequence of this for the embedding energies will be discussed later. During all fits the potential parameters for the zeolite from Ref. [39] were kept without any changes. The final parameter adjustments were done on NH_3 and NH_4^+ adsorbed on a tri-tetrahedra cluster. The potential parameters are listed in Table 2.

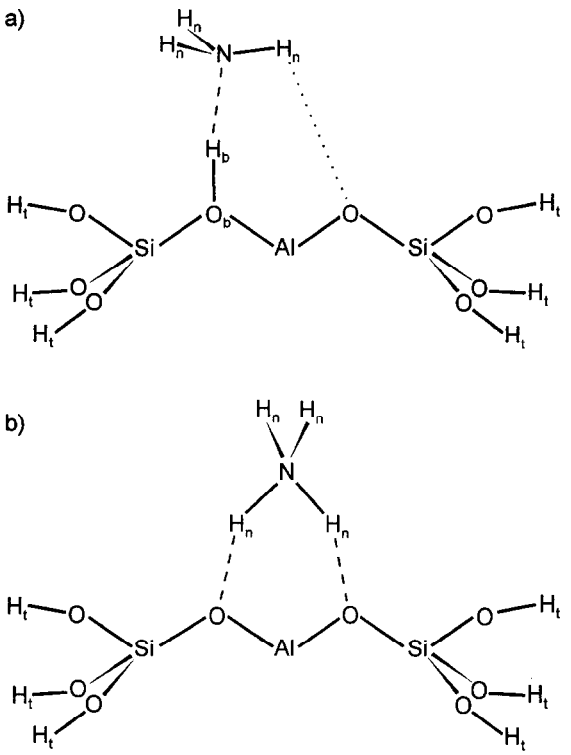

Fig. 2. Definitions of the ion types used in the ab initio shell model potential for the interaction of NH_3 and NH_4^+ with the zeolite frameworks demonstrated for the T3-model. The ion types for the zeolite were already defined in [39]. (a) NH_3, (b) NH_4^+.

2.5. Embedding calculations

In all embedding calculations on faujasite a reduced, triclinic unit cell containing 48 T atoms with Si/Al = 47 was used. NH_3 was placed onto a bridging hydroxyl group at O1 or O4, and NH_4^+ was positioned in 2-coordination over O1 and O4. The initial structures were then generated by constant pressure lattice energy minimization of all atom positions with the

Table 1
Ab initio data base for the NH_3/NH_4^+–zeolite interaction potential fits

Pot	Model	SCF energy (au)	Symmetry	Stationary point
NH_3	NH_3	−56.20563	C_{3v}	minimum
	$Al(OH)_4H \cdot NH_3$	−600.77054	C_s	SP4 [b]
	$(HO)_3Si–O(H)–Al(OH)_2–O–Si(OH)_3 \cdot NH_3$	−1630.68183	C_s	SP3 [b]
NH_4^+	NH_4^+	−56.55087	T_d	minimum
	$Al(OH)_4^- \cdot NH_4^+$ [a]	−600.77241	C_1	minimum
	$(HO)_3Al–O–Si(OH)_3^- \cdot NH_4^+$	−1115.69875	C_s	SP3 [b]
	$(HO)_3Si–O–Al(OH)_2–O–Si(OH)_3^- \cdot NH_4^+$	−1630.69134	C_{2v}	SP5 [b]
	$(HO)_3Si–O–Al(OH)_2–O–Si(OH)_3^- \cdot NH_4^+$	−1630.67821	C_s	SP3 [b]

[a] Ref. [1].
[b] SPn – saddle point of nth order.

potentials described in the preceding section, which are the same used for the embedding calculations. This has the advantage that the structures for the embedding calculations are already nearly converged for the part of the system that is described by the potential only. For all shell model calculations we used the program GULP [40]. The protonated structures at O1 and O4 were taken from [39]. The structure of the deprotonated zeolite was obtained by immersing the negatively charged framework into a neutralizing homogeneous background charge distribution (jellium). For this, the necessary compensating term in the Ewald energy [41,42] and its derivatives with respect to the strains [30] were implemented into the GULP program [40].

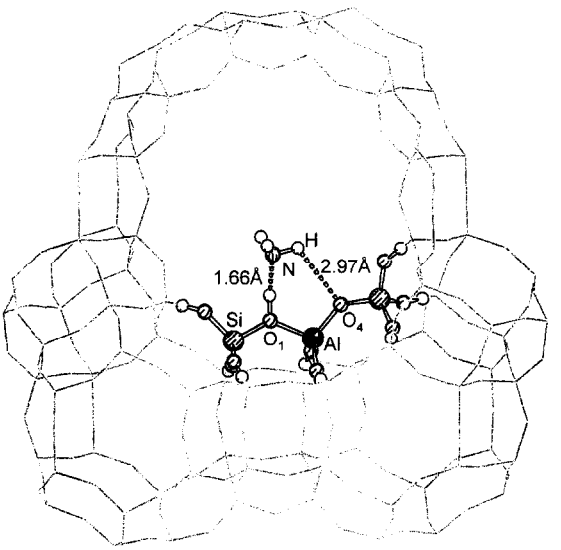

Fig. 3. Tri-tetrahedra model with adsorbed ammonia embedded at O1 in tile supercage of faujasite. Similar models were embedded for the Y^-, H–Y, and NH_4–Y zeolites.

Table 2
Parameters of the ab initio shell model potential for the interaction of zeolites with NH_3 and NH_4^+

	Charges (e)			
	zeolite–NH_3		zeolite–NH_4^+	
	core	shell	core	shell
N	1.49428	−4.49428	−3.0	—
H_n	1.0	—	1.0	—
	Short range repulsion			
	zeolite–NH_3		zeolite–NH_4^+	
	A (eV)	ρ (Å)	A (eV)	ρ (Å)
N–H_n	429.79968	0.25508	408.71064	0.25315
Si–N	756.03094	0.42789	2464.75068	0.24705
Al–N	1192.26541	0.44023	1188.31660	0.26794
H_n–O	2308.56712	0.24161	3016.78651	0.20739
H_n–O_b	916.49785	0.21288	—	—
H_b–N	605.56450	0.27092	—	—
	Core–shell interaction			
	zeolite–NH_3		zeolite–NH_4^+	
	k (eV Å^{-2})		k (eV Å^{-2})	
N	191.46559		—	
	Three-body interaction			
	zeolite–NH_3		zeolite–NH_4^+	
	k [b] (eV rad^{-2})	θ_0 (deg)	k [b] (eV rad^{-2})	θ_0 (deg)
H–N–H	0.593524	107.04	—	—

A tri-tetrahedra model (T3 model) was embedded so that the two central oxygen atoms were at positions O1 and O4 around aluminum, see Fig. 3. The embedding calculations were carried out in constant volume with the cell constants as determined before and within spacegroup P1. The potential part and the QM part were combined using an implementation as described in Ref. [43] [2]. An energy threshold of 0.01 kJ/mol was taken as convergence criterion. In order to estimate the effect of the structure constraints exerted by the embedding on the reaction energies, free cluster optimizations of NH_3 and NH_4^+ adsorbed on a T3 model, the protonated T3 model itself and of its deprotonated form were also carried out. These structure optimizations were done in C_s symme-

[2] This implementation will be also made available as part of MSI's catalysis and sorption project.

try to avoid hydrogen bridging between neighboring terminal hydroxyl groups.

3. Results and discussion

3.1. Structures

Table 3 compares the NH_3 and NH_4^+ loaded structures obtained by the embedding procedure and by the shell model potential alone. The small differences of the structure parameters in the case of NH_3 indicate that the analytical interaction potential fits well to the ab initio results. As expected, the non-bonded $H_n \cdots O$ distance undergoes the largest change upon embedding. On both positions, O1 and O4, the ammonia molecule forms a non-linear bond with the bridging hydroxyl group, pointing with one of its hydrogen atoms to an aluminum bonded framework oxygen. Similar structures were found in cluster calculations [1,6,11]. The NH_4^+ ion is twofold coordinate on O1 and O4. The quality of the NH_4^+ potential is lower than that of the NH_3-potential. Whereas the differences in the H_n–O distances between potential and embedding structures are small, the quantum mechanical part in the embedding scheme had to correct the Al–O and N–H bond lengths that are involved in the adsorption of NH_4^+.

3.2. Reaction energies

For the discussion of the results, we decompose the proton transfer which converts the

Table 3
Bond lengths (Å) and angles (deg) of the NH_3- and NH_4^+-adsorbed models

	NH_3–T3 (O1)		NH_3–T3 (O4)		NH_4–T3 (O1, O4)	
	Embed	Pot [a]	Embed	Pot	Embed	Pot
Bond lengths						
Si–O1	1.678	1.677	1.594	1.590	1.610	1.608
Si–O4	1.584	1.585	1.663	1.676	1.598	1.603
Al–O1	1.867	1.877	1.723	1.741	1.781	1.813
Al–O2	1.702	1.695	1.714	1.708	1.718	1.710
Al–O3	1.724	1.719	1.717	1.714	1.729	1.724
Al–O4	1.710	1.729	1.851	1.865	1.762	1.796
O_b–H_b	1.007	0.993	1.013	0.998		
H_b–N	1.661	1.686	1.642	1.677		
O1–H_n			2.972	3.000	1.772	1.770
O4–H_n	2.972	2.889			1.800	1.790
N–H_n	1.013	1.013	1.009	1.021	1.033	1.047
	1.011	1.012	1.012	1.012	1.033	1.045
	1.008	1.022	1.014	1.014	1.008	0.994
					1.014	0.993
Bond angles						
Si–O1–Al	127	129	133	136	128	130
Si–O4–Al	137	139	131	132	133	133
Al–O_b–H_b	114	116	112	114		
O_b–H_b–N	176	174	178	176		
H_n–N–H_n	106	103	106	104	102	104
	106	103	106	103	110	111
	105	103	105	103	110	110
					110	112
					111	111

[a] From constant pressure lattice energy minimization with shell model potential, identical with start structure for embedding calculation.

neutral complex (NC) into the ion-pair structure (IP) into the following four steps:

– Desorption of the neutral molecule:

$$Z\text{–}OH \cdots B \rightarrow Z\text{–}OH + B \quad (11)$$

– Deprotonation of the acidic Brønsted site:

$$Z\text{–}OH \rightarrow Z\text{–}O^- + H^+ \quad (12)$$

– Protonation of the molecule:

$$B + H^+ \rightarrow BH^+ \quad (13)$$

– Formation of the ion-pair (IP) complex:

$$Z\text{–}O^- + BH^+ \rightarrow Z\text{–}O^- \cdots BH^+ \quad (14)$$

The reaction energy of the second step is the deprotonation energy, the corresponding Gibbs free energy of gas phase molecules is the acidity. It has been shown that the deprotonation energy directly calculated from the energy difference of $Z\text{–}O^-$ and Z–OH serves as a suitable quantum chemical measure of the acidity [44]. The proton affinity of the molecule B is defined by the reaction heat of Eq. (13). In the gas phase, the proton transfer energy depends only on the acid strength of the active site and on the proton affinity of the molecule being protonated and is given by the sum of the reaction heats (Eqs. (12) and (13)). For a heterogeneous reaction, however, the proton transfer energy is defined with respect to Eq. (15) and additionally involves the difference of the binding energies of the neutral and ionic complexes:

$$Z\text{–}OH \cdots B \rightarrow Z\text{–}O^- \cdots BH^+ \quad (15)$$

Microcalorimetry and temperature-programmed desorption measurements usually yield the heat of adsorption of the ionic substrate with respect to the neutral components:

$$Z\text{–}OH + B \rightarrow Z\text{–}O^- \cdots BH^+ \quad (16)$$

The adsorption energies of NH_3 on the neutral zeolite (Eq. (11), reverse) and the (hypothetical) interaction energy between NH_4^+ and the deprotonated zeolite (Eq. (14)) are given in Table 4 for the sites O1 and O4. The free cluster NH_3 adsorption energy is -67 kJ/mol. This value is in good accordance with calculations on clusters with similar size and applying basis sets of similar quality (cf. Table 17 in Ref. [1]). Upon embedding at O1, the QM adsorption energy for the cluster only gets smaller (in absolute terms) due to structural constraints exerted by the framework. The long range contribution increases the absolute value to yield a total adsorption energy of -81 kJ/mol. It seems that the structural relaxation possible in free cluster optimizations partially compensates for missing long range effects, since in both NH_3 and NH_4^+ sorption the free cluster adsorption energies and the total energies are close.

Table 4
Adsorption energy of ammonia and interaction energy of the ammonium ion with the negatively charged zeolite surface for a free and for a mechanically embedded T3-cluster (kJ/mol)

	ΔE		
	NH_3		NH_4^+
	O1 (O4)	O4 (O1)	O1, O4
Free cluster (QM//free)		−67.1	−447.2
Embedded cluster			
Structural distortion [a]	+13.9	+13.9	−58.5
QM//Emb [b]	−53.2	−53.2	−505.7
LR//Emb [b]	−28.2	−33.8	58.4
Total [b]	−81.4	−87.0	−447.3

[a] QM//Emb − QM//free.
[b] Defined in Eqs. (5) and (6).

Table 5 shows the calculated energies for Eqs. (11), (14)–(16). The deprotonation energies (Eq. (12)) are presented in Ref. [30]. The first two data columns refer to the gas phase and embedded T3 cluster results. The data of the last three columns will be discussed below. From experiment it is clear that the interaction of NH_3 with hydroxyl sites is so strong that NH_4^+ ions are formed. The negative adsorption energies (Eq. (15)) indeed indicate that NH_4^+ forms as stable surface species on both O1 and O4. Moreover, the negative proton transfer energies (Tables 5 and 6) imply that the NH_4^+ species is the more stable one. The proton transfer energies are larger for O4–H than for O1–H protons, which is in accordance with the fact

Table 5
Adsorption energies ΔE_{Ads} of ammonia (Eq. (11), reverse) and the ammonium ion (Eq. (14)), proton transfer energies ΔE_{PT} (Eq. (15)), and formation energies of $NH_4^+ \cdots Y^-$ (Eq. (16)) (kJ/mol), O1 position. Convergence with increasing cluster size in the mechanical embedding calculation

	ΔE				
	[SiO^{1}AlOSi]		4^3 (shell-3.0) [b]	4^5 [b]	shell-5.0 [b]
	free	embedded			
$H-Y + NH_3 \rightarrow NH_3 \cdots H-Y$					
ΔE_{QM}(C)	−67.1	−53.2	−56.0	−61.3	−64.6
$\Delta E_{LR//Emb}$ [a]		−28.2	−24.5	−17.6	−13.9
Total		−81.4	−80.5	−78.9	−78.5
$Y^- + NH_4^+ \rightarrow NH_4^+ \cdots Y^-$					
ΔE_{QM}(C)	−447.2	−505.7	−488.3	−496.0	−477.1
$\Delta E_{LR//Emb}$ [a]		58.4	38.3	48.3	30.9
Total		−447.3	−450.0	−447.8	−446.2
$NH_3 \cdots H-Y \rightarrow NH_4^+ \cdots Y^-$					
ΔE_{QM}(C)	−25.0	−5.1	−7.4	−6.7	−16.1
$\Delta E_{LR//Emb}$ [a]		−19.4	−19.5	−19.7	−11.0
Total		−24.5	−26.9	−26.3	−27.1
$H-Y + NH_3 \rightarrow NH_4^+ \cdots Y^-$					
ΔE_{QM}(C)	−92.1	−58.4	−63.4	−67.9	−80.7
$\Delta E_{LR//Emb}$ [a]		−47.5	−43.9	−37.3	−24.9
Total		−105.9	−107.4	−105.2	−105.6

[a] Defined in Eq. (6).
[b] 'Single point' calculations.

that binding of protons on O4 is weaker than on O1 [30,39] and with the low experimental occupation of O4 compared to O1 sites [45].

The long range potential contribution enhances the relative stabilization of NH_4^+. But the limited relaxation in the framework reduces it from −25 kJ/mol for the free to −5 kJ/mol for the embedded cluster (Table 5). The total embedded result is remarkably close to the free cluster result. As has been discussed in [1], ab initio calculations and other embedding schemes which apply smaller basis sets [28] often fail to describe the ion-pair as more stable than the neutral complex. The reason for this is that non-flexible basis sets, e.g. STO-3G, are not appropriate for describing the anion in the ion

Table 6
Effect of a change of the NH_3/NH_4–zeolite interaction potential onto the proton transfer energies ΔE_{PT} (kJ/mol) from the neutral complex to the ion pair calculated with mechanical embedding

ΔE_{PT}	O1 (O4)		O4 (O1)	
	present potential	old potential	present potential	old potential
$\Delta E_{Pot//Emb}$(S)	−99.8	−569.6	−116.1	−583.3
$\Delta E_{Pot//Emb}$(C)	−80.4	−548.5	−82.8	−552.1
$\Delta E_{LR//Emb}$ [a]	−19.4	−21.1	−33.3	−31.2
$\Delta E_{Pot//Emb}$(C)	−5.1	−4.0	−8.0	−9.5
Total	−24.5	−25.1	−41.4	−40.7

[a] Individual contributions defined in Eq. (5).
[b] Defined in Eq. (6), difference of the two rows above.

pair. In cluster calculations the ion pair structure is more stable provided that reasonable basis sets were applied and proper models were used [1]. The latter is the case if two or three protons of the ammonium ion are complexing the oxygen atoms bound to aluminum [1,5,6,9,10]. It is therefore important to choose basis sets which are suited to describe both the ionic and neutral components, e.g. the double zeta plus polarization basis sets. This is easily done in the present embedding scheme.

3.3. The problem of using different potentials for $ZOH \cdots NH_3$ and $ZO^- \cdots NH_4^+$

The embedding potentials for the adsorbate systems $ZOH \cdots NH_3$ and $ZO^- \cdots NH_4^+$ are different. Actually, the reaction energies ΔE do not vary much upon a change of the interaction potential from one side of the reaction to the other. This emerges from Table 6 which compares energies of proton transfer to ammonia (Eq. (15)) at O1 and O4 obtained with the present potential and with another potential of lower quality that has been derived by fits to hydrogen-saturated models. In this older potential also formal charges were assigned to the ion species. That these two potentials are different is clearly visible from the vastly different contributions of the host and cluster to the proton transfer energy. However, the long range contribution, defined as the difference between host and cluster potential energies (Eq. (6)), is nearly the same for both potentials. The remaining small differences are caused by structural changes due to the potentials applied. Why is this so? We look first at a situation which involves only one type of potential. This is the case for Eqs. (11) and (14). In addition to the existing zeolite potential they require only parameters for the interaction of the adsorbate with the zeolite framework and intramolecular terms. No change of atom types is involved. As discussed in Section 2.2, $\Delta E_{LR//Emb}$ contains electrostatic long range contributions only. As structural relaxations fade off fast with increasing distance from the reaction center, this long range contribution depends only on the charges of the atoms (and shell positions) in the outer region and in the adsorbate.

Consider now Eqs. (15) and (16) which involve both the potentials for $ZOH \cdots NH_3$ and $ZO^- \cdots NH_4^+$. A similar analysis as made above for the adsorption reactions (Eqs. (7a), (7b), (7c), (7d) and (8)) can be made for these reactions, which leads to the same result that $\Delta E_{LR//Emb}$ always contains only Coulombic interactions. A change of potentials does not influence the electrostatic long range contribution to the reaction energies much as long as the potentials use the same atom charges. In conclusion, we can take $\Delta E_{Pot//Emb}(S) - \Delta E_{Pot//Emb}(C)$ as an estimate of the long range contributions for all reactions described before.

3.4. Long range contributions

The long range contribution of the potential to the reaction energies for the embedded T3 clusters (second data rows in Table 5) is considerable, about 35% or -28.2 kJ/mol in the case of ammonia sorption at O1 (Eq. (11)) and 45% or -47.5 kJ/mol for NH_4^+ formation from the neutral gas phase species (Eq. (16)). We expected this potential term to decline and the quantum mechanical part to grow with increasing size of the embedded cluster. The stability of the actual QM/Pot result with increasing cluster size would provide strong support for the soundness of our method. Therefore, we used clusters of increasing size to check the convergence behavior. For the larger clusters we did not optimize the structure but performed 'single point' calculations using the structures obtained when embedding the T3 models. First, the T3 cluster was extended by completing three shells of silicon and oxygen atoms around the central aluminum atom (shell-3.0). If two terminating hydroxyl groups were pointing to the same silicon atom of the outer region, this silicon atom was also used in the cluster description and terminated with hydroxyl groups. Shell-3.0 is

therefore equivalent to three connected 4-rings, 4^3. Adding another two shells of silicon and oxygen atoms yields the shell-5.0 model which is rather large (about 1800 basis functions). An intermediate model between shell-3.0 and shell-5.0 is the 4^5 model which includes four coordination shells around the O1–Al–O4 group. The 4^5 notation points to the fact that 5 4-rings are present. The models are shown in Fig. 4. Calculations were made on these clusters at the structure obtained from the embedded structure optimizations which used the tri-tetrahedra models at O1 as the quantum part, i.e., single point shell model potential and HF calculations were made without relaxing the structure.

Table 5 shows the results. Although the long range contributions of the potential converge slowly, the total QM/Pot energies are remarkably stable with increasing cluster size. For the adsorption energies of NH_3 and NH_4^+ from the neutral gas phase species, Eq. (11) (reverse) and Eq. (16), respectively, the long range part decreases in favor of the quantum part by about 14 and 22 kJ/mol, respectively, while the total QM/Pot results stay the same within 3 kJ/mol. Large steps downwards of the long range contribution occur from the 4^3 to the 4^5, and from the 4^5 to the shell-5.0 models.

3.5. Effect of electron correlation and comparison with previous work

Our calculated QM/Pot adsorption energies of the ammonium ion with respect to the neutral components are about 105–107 kJ/mol in the case of O1 and around 128 kJ/mol at O4. Since electron correlation effects are missing, they were now taken into account by applying a perturbative correction at the MP2 level to the embedded T3 clusters and to the free ammonia. The basis set superposition error (BSSE) was calculated with the full counterpoise correction (CPC) according to Boys and Bernardi [46]. Table 7 lists the results. Electron correlation increases the binding energy of NH_4^+ by about 30 kJ/mol. The effect of the BSSE is small and

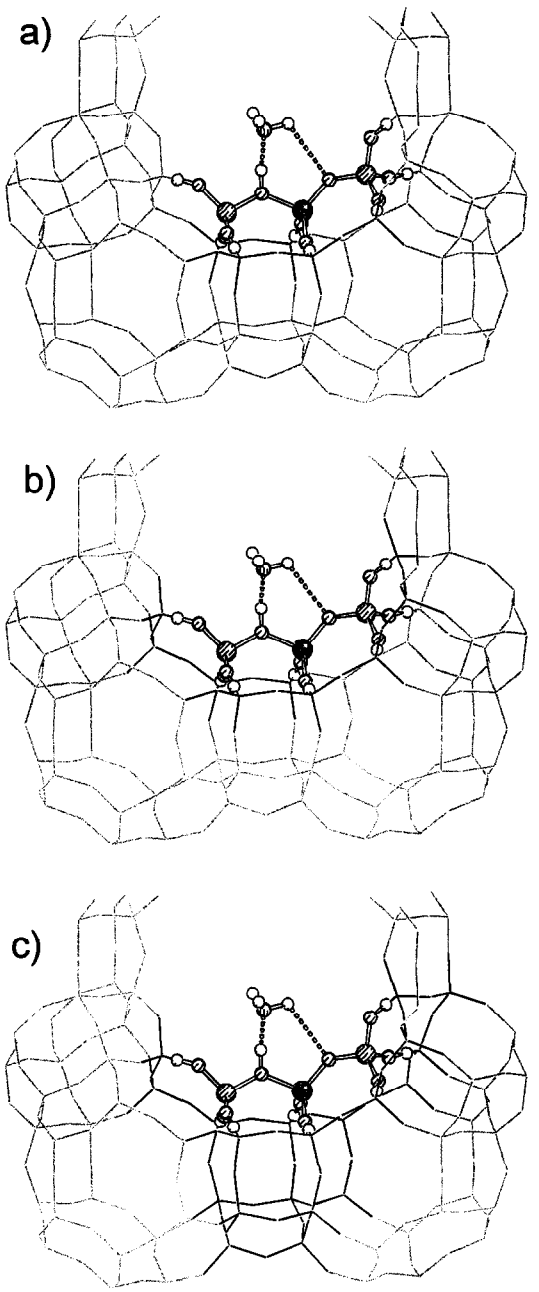

Fig. 4. Clusters of increasing size embedded into the faujasite structure for convergence tests. The dark lines indicate the cluster. (a) 4^3 (shell-3.0), (b) 4^5, (c) shell-5.0 model. Similar models were embedded for the Y^-, H–Y, and NH_4–Y zeolites.

reduces the binding energy by about 14 kJ/mol. In the case of O1 we obtain a final formation energy of NH_4^+ of 123 kJ/mol.

Embedding calculations on ammonia sorption

on H-faujasite were also carried out by Greatbanks et al. [26]. In their work, they embedded hydrogen terminated T3 clusters into a lattice of point charges that were fitted to the periodic electrostatic potential of a siliceous faujasite calculated at the Hartree–Fock level. A 3-21G basis set was employed in the periodic calculations. The cluster calculations were carried out by the MP2 method using a 6-31G** basis set. The formation energies of NH_4^+ from the neutral components are somewhat larger than our values (Table 7). As in our calculations, the binding of NH_4^+ is favored over that of NH_3. Unfortunately, the paper does not mention to which oxygen positions the NH_3/NH_4^+ species were attached. Contrary to our results, large changes of the H_n–O distances of 0.4–0.7 Å were observed after embedding into the point charge lattice and a single and short H_n–O bond from the NH_4^+ ion to the zeolite is preferred. This structure is different from the structure we found. These differences are probably due to the restricted optimization which with Greatbanks et al.'s type of embedding scheme was possible only for the $AlO_4(H)$ core and the adsorbate. Other MP2 results (Table 7) were obtained for a different framework (chabazite CHA) [18] or for a free space cluster [6]. The former used a structure which was only partially relaxed and was affected by a large BSSE [18].

3.6. Final estimates and comparison with experiments

The comparison of calculated formation energies of NH_4^+ in zeolites with experiment is difficult, since microcalorimetry and temperature-programmed desorption experiments on a number of H–Y zeolites prepared under different conditions give a large range of adsorption energies between 90 and 180 kJ/mol [47–51]. The higher adsorption energies between 130 and 180 kJ/mol are generally attributed to strong Lewis acid sites which are generated during dehydroxylation and its accompanying dealumination of the zeolite [47,49]. It was also suggested that the presence of non-framework aluminum species might influence the acid strength of neighboring Brønsted acid sites [47]. For the strong Brønsted acid sites between 100 and 130 kJ/mol it was observed that the heat of adsorption increases with increasing Si/Al ratio [49,50]. Deconvolutions of the TPD spectra of HNa–Y with a suitable distribution function yielded 78–96 kJ/mol for medium Brønsted sites and 104–111 kJ/mol for strong sites depending on the aluminum content (Si/Al = 2.4–5.8) [49]. Similar values of 91, 101, and 111 kJ/mol were obtained on HNa-Y with Si/Al 2.6 [51]. In combination with IR spectroscopic measurements, the latter value of 111

Table 7
Comparison of adsorption energies calculated at a correlated level of NH_4^+ on zeolite models with respect to the neutral components (kJ/mol)

Model	Structure	Method	$-\Delta E$	Ref.
T3	FAU, O1	MP2//SCF/TZ(O, N)DZP	137	this work
		MP2/CPC//SCF/TZ(O, N)DZP	123	
$H_3SiO(H)Al(OH)_2OSiH_3$	FAU [a,b]	MP2//SCF/6-31G**	145	[26]
		MP2/CPC [c]//SCF/6-31G**	125–133	
$Si_6Al_2O_{10}H_{16}$	CHA [d,b]	MP2/6-31G(d) [e]	113	[18]
		MP2/CPC/6-31G(d) [e]	51	
$H_3SiO(H)Al(H_2)OSiH_3$	free	MP2//SCF/6-31G*	105	[6]
		MP2/6-31G	112	

[a] Embedded into point charges fitted to ESP of the crystal calculated with SCF/3-21G.
[b] Only AlO_4 and NH_4^+ relaxed.
[c] BSSE estimated from SCF-BSSE given in Ref. [26].
[d] External electrostatic potential of the crystal added to Fock matrix.
[e] Si, Al: 6-31G(d), O_b: 6-311G(d), O, N: 6-31G, H_b, H_n: 3-1G, H_t: STO-3G.

kJ/mol was assigned to ammonia adsorbed on the HF protons at O1 and O4. Diffential heat of adsorption curves obtained by microcalorimetry on carefully dealuminated faujasites (Si/Al = 5.6) show an onset between 120 and 130 kJ/mol for initial coverage of Brønsted sites with ammonia [50]. Our calculated value, 123 kJ/mol, still needs corrections for zero point energy (ZPE) and thermal contributions before comparison can be made with experiments. From previous SCF calculations on a H-saturated pentameric cluster (shell-2) [1] values of +16 and +11 kJ/mol are known for ΔZPE and $\Delta\Delta H(T)$, respectively. The final estimate, 112 kJ/mol, falls into the lower part of the experimental range of 110–130 kJ/mol.

4. Conclusions

We have shown that the QM/MM scheme which proved successful in the description of crystalline silica polymorphs [29] and acidic zeolites [30] can be extended to the description of zeolite–adsorbate interactions. As a demonstrative application we chose ammonia adsorption in faujasite. Shell model potentials based on ab initio data had to be developed for the interaction of ammonia and ammonium ions with zeolites. Although these are of lower quality than the ab initio shell model potentials developed for zeolite frameworks, they yield reasonable start structures for embedding calculations. Final structures after optimization with the embedding scheme agree well with the start structures derived with the NH_3/NH_4^+ potentials only.

The main potential of the present embedding scheme is that relaxation of the host matrix is included which accommodates adsorbate induced distortions. This is an advantage compared with other schemes which embed the cluster into a charge or multipole distribution and permit structure optimization only for the part that does not overlap with the external electrostatic potential of the crystal [26]. The long range contribution to the reaction energies is easily obtained in our scheme as the difference of the MM energies of the host (periodic lattice) and the embedded cluster. Although its contribution to the adsorption energy of NH_4^+ is considerable, and although it decreases slowly with increasing cluster size, the final QM/Pot result is remarkably stable. The large structural relaxation effects of free space clusters seem to compensate partially for neglected long range effects.

Our scheme easily allows to use basis sets which are sufficiently large and flexible to describe both the neutral complex and the ion pair structures well. Ammonium ions in zeolites are therefore correctly described as more stable than ammonia. Electron correlation can be also included. After doing this, the formation energy calculated for NH_4^+ from O1–H falls into the range provided by temperature-programmed desorption and microcalorimetry of ammonia on H-faujasites.

The present QM/Pot embedding scheme is able to discriminate between different catalytically active sites, shown here for ammonia adsorption and deprotonation at oxygen positions O1 and O4 in faujasite.

Acknowledgements

We thank J. Gale (London) and R. Ahlrichs (Karlsruhe) for providing recent versions of the GULP and TURBOMOLE codes, respectively. M.B. gratefully acknowledges a grant from the Alexander-von-Humboldt foundation and thanks U. Eichler and K.-P. Schröder for helpful discussions. This work has been supported by the "Fonds der Chemischen Industrie" and by a consortium of industrial and academic members within the catalysis and sorption project of Molecular Simulations Inc.

References

[1] J. Sauer, P. Ugliengo, E. Garrone and V.R. Saunders, Chem. Rev. 94 (1994) 2095.
[2] W.E. Farneth and R.J. Gorte, Chem. Rev. 95 (1995) 615.
[3] H.V. Brand, L.A. Curtiss and L.E. Iton, J. Phys. Chem. 96 (1992) 7725.
[4] E.H. Teunissen, W.P.J.H. Jacobs, A.P.J. Jansen and R.A. van Santen, in: R. von Ballmoos et al. (Eds.), Proc. of the 9th Int. Zeolite Conf., Montreal 1992, Butterworth-Heinemann, 1993, p. 469.
[5] E.H. Teunissen, R.A. van Santen, A.P.J. Jansen and F.B. van Duijneveldt, J. Phys. Chem. 97 (1993) 203.
[6] E. Kassab, J. Fouquet, M. Allavena and E.M. Evleth, J. Phys. Chem. 97 (1993) 9034.
[7] J. Sauer, Chem. Rev. 89 (1989) 199.
[8] J. Sauer, in: C.R.A. Catlow (Ed.), Molecular Modelling of Structure and Reactivity in Zeolites, Academic Press, London, 1992, p. 183.
[9] J. Sauer, C. Kölmel, F. Haase and R. Ahlrichs, in: R. von Ballmoos et al. (Eds.), Proc. of the 9th Int. Zeolite Conf., Montreal 1992, Butterworth-Heinemann, 1993, p. 679.
[10] J. Sauer, Stud. Surf. Sci. Catal. 84 (1994) 2039.
[11] F. Haase and J. Sauer, J. Phys. Chem. 98 (1994) 3083.
[12] F. Haase and J. Sauer, J. Am. Chem. Soc. 117 (1995) 3780.
[13] M. Krossner and J. Sauer, J. Phys. Chem. 100 (1996) 6199.
[14] J. Sauer, Science 271 (1996) 774.
[15] E.H. Teunissen, C. Roetti, C. Pisani, A.J.M. de Man, A.P.J. Jansen, R. Orlando, R.A. van Santen and R. Dovesi, Mod. Simul. Mater. Sci. Eng. 2 (1994) 921.
[16] C. Pisani, R. Dovesi and C. Roetti, Lecture Notes in Chemistry, Vol. 48. Hartree–Fock Ab Initio Treatment of Crystalline Systems, Springer, Berlin, 1988.
[17] E.H. Teunissen, A.P.J. Jansen, R.A. van Santen, R. Orlando and R. Dovesi, J. Chem. Phys. 101 (1994) 5865.
[18] E.H. Teunissen, A.P.J. Jansen and R.A. van Santen, J. Phys. Chem. 99 (1995) 1873.
[19] E. Nusterer, P.E. Blöchl and K. Schwarz, Angew. Chem. 108 (1996) 187.
[20] E. Nusterer, P.E. Blöchl and K. Schwarz, Chem. Phys. Lett. 253 (1996) 448.
[21] R. Shah, M.C. Payne, M.-H. Lee and J.D. Gale, Science 271 (1996) 1395.
[22] C. Pisani, F. Corà, R. Nada and R. Orlando, Comput. Phys. Commun. 82 (1994) 139.
[23] C. Pisani, S. Casassa and F. Corà, Comput. Phys. Commun. 82 (1994) 157.
[24] C. Pisani and F. Corà, Comput. Phys. Commun. 82 (1994) 168, 179, 187.
[25] S.P. Greatbanks, P. Sherwood and I.H. Hillier, J. Phys. Chem. 98 (1994) 8134.
[26] S.P. Greatbanks, P. Sherwood, I.H. Hillier, R.J. Hall, N.A. Burton and I.R. Gould, Chem. Phys. Lett. 234 (1995) 367.
[27] A. Kyrlidis, S.J. Cook, A.K. Chakraborty, A.T. Bell and D.N. Theodorou, J. Phys. Chem. 99 (1995) 1505.
[28] C. Pisani and U. Birkenheuer, Int. J. Quant. Chem.: Quant. Chem. Symp. 29 (1995) 221.
[29] U. Eichler, C.M. Kölmel and J. Sauer, J. Comput. Chem., in press.
[30] U. Eichler, M. Brändle and J. Sauer, in preparation.
[31] H.G. Karge, in: G. Öhlmann et al. (Eds.), Catalysis and Adsorption by Zeolites, Elsevier, Amsterdam, 1991, p. 133.
[32] W.P.J.H. Jacobs, J.W. de Haan, L.J.M. van de Ven and R.A. van Santen, J. Phys. Chem. 97 (1993) 10934.
[33] R. Ahlrichs, M. Bär, M. Häser, H. Horn and C. Kölmel, Chem. Phys. Lett. 162 (1989) 165.
[34] S. Huzinaga, Approximate atomic wavefunctions I, II (University of Alberta, Edmonton, 1971).
[35] S. Huzinaga, J. Chem. Phys. 42 (1965) 1293.
[36] B.G. Dick and A.W. Overhauser, Phys. Rev. 112 (1958) 90.
[37] J.-R. Hill and J. Sauer, J. Phys. Chem. 98 (1994) 1238.
[38] J.-R. Hill and J. Sauer, J. Phys. Chem. 99 (1995) 9536.
[39] K.-P. Schröder and J. Sauer, J. Phys. Chem. 100 (1996) 11043.
[40] J.D. Gale, Program GULP (General Utility Lattice Program) (Royal Institution/Imperial College, UK, 1992–1994).
[41] M. Leslie and M.J. Gillan, J. Phys. C: Solid State Phys. 18 (1985) 973.
[42] K. Fuchs, Proc. Roy. Soc. A 151 (1935) 585.
[43] U. Eichler, Ph.D. Thesis, Humboldt-Universität zu Berlin, in preparation.
[44] J. Sauer, J. Molec. Catal. 54 (1989) 312.
[45] M. Czjzek, H. Jobic, A.N. Fitch and T. Vogt, J. Phys. Chem. 96 (1992) 1535.
[46] S.F. Boys and F. Bernardi, Mol. Phys. 19 (1970) 553.
[47] R.D. Shannon, K.H. Gardner, R.H. Staley, G. Bergeret, P. Gallezot and A. Auroux, J. Phys. Chem. 89 (1985) 4778.
[48] D.J. Parrillo and R.J. Gorte, J. Phys. Chem. 97 (1993) 8786.
[49] H.G. Karge, V. Dondur and J. Weitkamp, J. Phys. Chem. 95 (1991) 283.
[50] U. Lohse, B. Parlitz and V. Patzelová, J. Phys. Chem. 93 (1989) 3677.
[51] B. Hunger and M. v. Szombathely, Z. Phys. Chem. 190 (1995) 19.